




**Controllable wrinkling in a prestretched dielectric elastomer sheet with striped electrodes**Peibao Xu <sup>\*</sup>, Jieli Jin , and Kai Li *Department of Civil Engineering, Anhui Jianzhu University, Hefei, Anhui 230601, People's Republic of China*

(Received 5 February 2021; revised 27 April 2021; accepted 19 May 2021; published 7 June 2021)

Controllable wrinkling of dielectric elastomer (DE) sheets is often applied to achieve some special applications such as diffraction gratings, optical sensors, soft actuators, and adjustable wetting surfaces. It is required to precisely predict and control the threshold voltage and wavelength of wrinkling. In view of the weakness of loss of tension criterion, a nonlinear plate theory considering the bending energy of DE sheet is utilized to investigate the wrinkling phenomenon in a prestretched DE sheet with striped electrodes. The results show that the threshold voltage of wrinkling is bigger than the corresponding voltage obtained from loss of tension, which results from the fact that the bending energy has a certain inhibiting effect on wrinkling of the DE sheet. Furthermore, the threshold voltage and wavelength of wrinkling can be effectively regulated by controlling prestretch. The striped electrodes can also effectively control the threshold voltage and wavelength. Especially, there exists an optimal width ratio of electrode corresponding to the lowest threshold voltage. The proposed method can be used to predict and control the behavior of wrinkling in the engineering applications of DE structures.

DOI: [10.1103/PhysRevE.103.063001](https://doi.org/10.1103/PhysRevE.103.063001)**I. INTRODUCTION**

Dielectric elastomer (DE) is a kind of electroactive polymer, and has a lot of excellent features such as being light weight, having high energy density, large deformation, fast response, low cost, and good flexibility [1–3]. The DE sheet can produce large deformation under the action of an electric field [4]. Based on this principle, the DE sheet can be used to design and manufacture transducers, smart actuators, flexible sensors, and soft robots [3], etc. Currently, the DE sheet has got certain applications in many fields, such as crawling robots [5], artificial eyes [6,7], energy harvesters [8], and soft grippers [9].

In order to achieve large deformation at relatively low voltage, the DE material is often fabricated into a thin film structure. In this case, the DE sheet is more prone to wrinkle under the action of the same electric field. The wrinkling phenomenon is often thought to be a form of DE sheet failure [10–15], which should be avoided as much as possible in practical application. Meanwhile, the wrinkling phenomenon in some cases can recover without causing any damage [16,17]. In addition, the wrinkling phenomenon of DE sheet is also used to achieve some special applications such as diffraction gratings [18], optical sensors [19], and adjustable wetting surfaces [20].

In order to analyze the critical conditions for DE sheet wrinkling, the instability criterion of loss of tension is often used to predict the critical voltage [21–25]. Generally, the DE sheet is very thin and its bending energy is small, therefore, the loss of tension in the DE sheet under the action of electric field is considered as the critical condition for wrinkling [24]. This criterion is simple and the theoretical prediction results are in good agreement with the experimental results in many cases [21–26]. Although this criterion can approximately

estimate the critical condition of wrinkling, the important results such as the wavelength of wrinkling cannot be obtained due to ignoring bending energy [27]. The applications of DE sheet in many fields such as soft robot and artificial eye all require the precise control of its critical voltage and wavelength of wrinkling. Recently, the DE plate theory considering bending energy has attracted much attention [27–30]. A DE plate theory was developed to study the wrinkling critical voltage and wavelength of the annular sheet, and the theoretical prediction was consistent with the experimental results [27]. Based on the wavelength obtained by nucleation theory, the post-buckling of the DE sheet was analyzed by an energy method considering bending energy, stretching energy, and electric field energy to predict wrinkling amplitude [28]. A theoretical model is developed to predict the wrinkling wavelength, post-buckling amplitude, and critical wrinkling voltage of the substrate-free membrane [29]. A model of the wrinkled plate is established and provides good estimates of the critical voltage and wave number of wrinkles [30].

The above theories have been applied in the cases of DE sheets with full coated electrodes. Recently patterned electrodes are used in applications of the DE sheet to achieve a variety of instability morphologies [27]. In this work, we explore the wrinkling behavior and mechanism of a system of DE sheet with striped electrodes, and focus on the effect of the width ratio of striped electrodes and prestretches, by considering the bending, stretching, and electric field energy, which is different from the loss of tension criterion. To regulate deformation and wrinkling of DE sheet with patterned electrodes, based on the nonlinear plate theory, a model considering the prestretch and striped electrodes is developed, and wrinkling behaviors of the DE sheet is extensively studied in this paper. The rest of the paper is organized as follows. In Sec. II, a nonlinear plate model for the DE sheet is formulated and linear stability analysis of the DE sheet with striped electrodes is conducted. In Sec. III, the prebuckling stress fields are

<sup>\*</sup>Corresponding author: peibaouxu@ahjzu.edu.cn

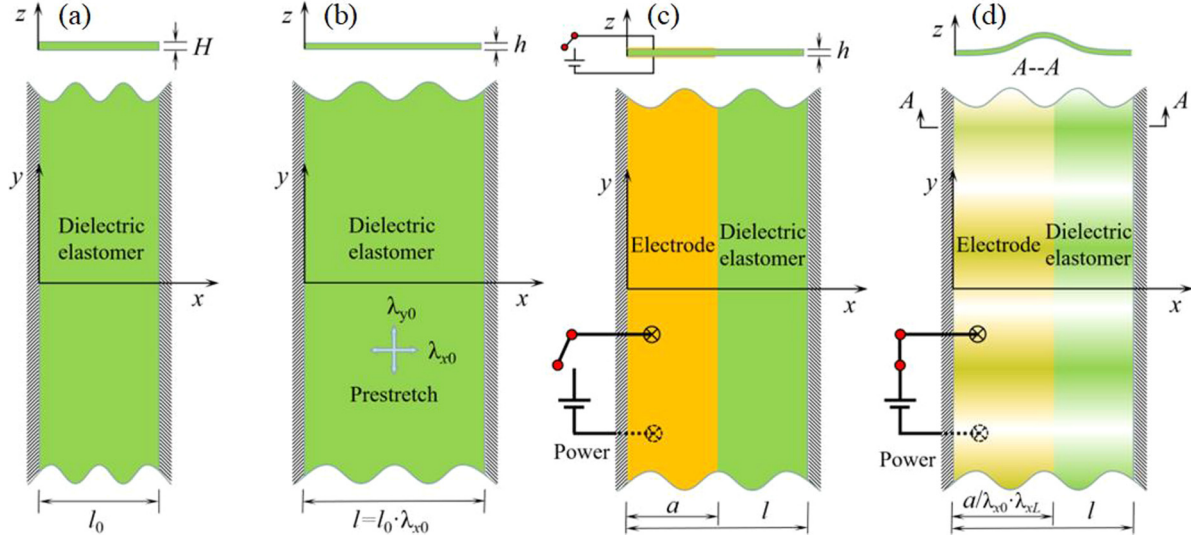


FIG. 1. Schematic diagram of a DE sheet with two ends clamped by rigid fixtures: (a) A DE sheet with initial length  $l_0$  and thickness  $H$  in the reference state; (b) the DE sheet with prestretches  $\lambda_{x0}$  and  $\lambda_{y0}$  along the  $x$ -axis and  $y$ -axis directions, respectively, and current thickness  $h$ ; (c) the DE sheet coated with carbon grease as electrodes on the left side of width  $a$  in the undeformed state without wrinkling and (d) the wrinkling state of DE sheet. The DE sheet will generate wrinkles when the applied voltage  $\Phi$  is on and large enough. In the current state, the stretches of the coated carbon grease and without grease regions are  $\lambda_{xL}$  and  $\lambda_{xR}$ , respectively.

given and then the effects of width ratio and prestretch on the critical condition and mode of wrinkling are investigated. The concluding remarks are given in Sec. IV.

## II. MODEL AND THEORETICAL FORMULATION

### A. Prebuckling analysis for a prestretched DE sheet with striped electrodes

Two ends of a DE sheet are clamped by two rigid fixtures, and a Cartesian orthogonal coordinate system  $(x, y, z)$  is adopted, where the  $z$  axis is normal to the DE plane as shown in Fig. 1. The initial state is regarded as the reference state as shown in Fig. 1(a), in which the thickness of DE sheet is  $H$  and its length along the  $x$  axis is  $l_0$ , while the length along the  $y$  axis can be seen as infinite. Subsequently, the DE sheet will be prestretched along the  $x$ -axis and  $y$ -axis directions and the prestretches are  $\lambda_{x0}$  and  $\lambda_{y0}$ , respectively. Under the action of prestretching, the thickness of DE sheet changes into  $h$  uniformly as shown in Fig. 1(b). In this state, the left side of DE sheet is coated with carbon grease as the electrode and the coated width is  $a$  as shown in Fig. 1(c). In the actuated state, the electrical voltage  $\Phi$  is applied on the two surfaces of DE sheet. When the applied voltage is large enough, the wrinkles will nucleate and grow in the DE sheet as illustrated in Fig. 1(d). At this state, the current stretches of the coated carbon grease and without grease regions are  $\lambda_{xL}$  and  $\lambda_{xR}$ , respectively. In the following, the deformation of DE sheet without wrinkles will be analyzed first. Then, we theoretically analyze the nucleation of the wrinkle for the DE sheet subjected to a certain voltage.

In the initial state, i.e., the reference state, each material particle in the DE sheet along the  $x$ -axis and  $y$ -axis directions will be denoted by coordinates  $X$  and  $Y$ , respectively. In the wrinkling state, the position of the particles  $X$  and  $Y$  can be described by the functions of  $x(X)$  and  $y(Y)$ , respectively.

The stretches along the  $x$ -axis and  $y$ -axis directions can be described as

$$\lambda_x = \frac{dx}{dX}, \quad \lambda_y = \frac{dy}{dY}. \quad (1)$$

Generally, the DE material is assumed to be incompressible. Thus, the stretch along the  $z$ -axis direction is  $\lambda_z = 1/\lambda_x\lambda_y$ .

The electric field intensity  $E$  along the  $z$ -axis direction for the DE sheet can be calculated

$$E = \frac{\Phi}{h}, \quad (2)$$

where  $h = H\lambda_z$ .

The force balance equation along the  $x$ -axis direction in the DE sheet can be given as

$$\frac{\partial}{\partial x} \left( \frac{\sigma_{xx}}{\lambda_x} \right) = 0. \quad (3)$$

Based on the assumption of the ideal DE model, the permittivity  $\varepsilon$  is assumed to be constant, which is not affected by deformation and electric field [31]. Hereon, the free energy function  $W_s(\lambda_x, \lambda_y, \lambda_z)$  for the neo-Hookean hyperelastic model is given as

$$W_s = \frac{\mu}{2} (\lambda_x^2 + \lambda_y^2 + \lambda_z^2 - 3). \quad (4)$$

Thus the constitutive relations for DE material can be obtained by Ref. [32]

$$\begin{aligned} \sigma_{xx} &= \frac{\partial W_s(\lambda_x, \lambda_y, \lambda_z)}{\lambda_y \lambda_z \partial \lambda_x} - \varepsilon E^2, \\ \sigma_{yy} &= \frac{\partial W_s(\lambda_x, \lambda_y, \lambda_z)}{\lambda_x \lambda_z \partial \lambda_y} - \varepsilon E^2. \end{aligned} \quad (5)$$

Considering the incompressible condition of  $\lambda_z = 1/\lambda_x\lambda_y$ , substituting Eq. (4) into Eq. (5) leads to

$$\begin{aligned}\sigma_{xx}^L &= \mu(\lambda_{xL}^2 - \lambda_{xL}^{-2}\lambda_y^{-2}) - \varepsilon E^2, \\ \sigma_{xx}^R &= \mu(\lambda_{xR}^2 - \lambda_{xR}^{-2}\lambda_y^{-2}),\end{aligned}\quad (6a)$$

$$\begin{aligned}\sigma_{yy}^L &= \mu(\lambda_y^2 - \lambda_{xL}^{-2}\lambda_y^{-2}) - \varepsilon E^2, \\ \sigma_{yy}^R &= \mu(\lambda_y^2 - \lambda_{xR}^{-2}\lambda_y^{-2}),\end{aligned}\quad (6b)$$

where the term of  $-\varepsilon E^2$  is the well-known Maxwell stress caused by the electric field,  $\sigma_{xx}^L$ ,  $\sigma_{xx}^R$ ,  $\sigma_{yy}^L$ , and  $\sigma_{yy}^R$  are local stresses, in which  $L$  indicates the left part of DE sheet with coated carbon grease and  $R$  indicates the right part of DE sheet without coated carbon grease.

According to the balance Eq. (3), one can get the following relation:

$$\frac{\sigma_{xx}^L}{\lambda_{xL}} = \frac{\sigma_{xx}^R}{\lambda_{xR}}. \quad (7)$$

In order to obtain the solution of Eq. (7), there still need a supplementary equation, i.e., the deformation compatibility equation

$$\lambda_{xL}a + \lambda_{xR}(l - a) = \lambda_{x0}l. \quad (8)$$

With the help of Eq. (8), we can easily obtain the current stretches and stresses in the DE sheet by solving Eq. (7).

### B. Linear stability analysis for the DE sheet

To investigate the wrinkling phenomenon of DE sheet, a nonlinear plate theory is introduced to establish the governing equations of striped DE sheet subjected to the electromechanical loading. In the derivation of theoretical formulas, the relationships between the stress and deflection  $w = w(x, y)$  in the  $z$ -axis direction will be derived firstly for a striped DE sheet based on the neo-Hookean model [33] and Kirchhoff's hypotheses [34]. Then, the bending moment and twisting moment are further derived, and the force balance condition provides the governing equation for the wrinkling of the DE sheet.

For the sake of simplicity, the deformation gradient from the reference state  $\mathbf{B}_r$  to prestretched state  $\mathbf{B}_p$  is used to describe the deformation of the DE sheet when it is subjected to a homogeneous electric field along the  $z$ -axis direction. So one can obtain

$$\mathbf{F}_0 = \text{diag}(\lambda_x, \lambda_y, \lambda_z). \quad (9)$$

In the following, the displacement field will be represented by  $u$ ,  $v$ , and  $w$  in the three orthogonal directions  $x$ ,  $y$ , and  $z$ . At this moment, the deformation gradient from the prestretched state  $\mathbf{B}_p$  to the wrinkled state  $\mathbf{B}_w$  can be given by

$$\mathbf{F}_1 = \begin{bmatrix} 1 + \frac{\partial u}{\partial x} & \frac{\partial u}{\partial y} & \frac{\partial u}{\partial z} \\ \frac{\partial v}{\partial x} & 1 + \frac{\partial v}{\partial y} & \frac{\partial v}{\partial z} \\ \frac{\partial w}{\partial x} & \frac{\partial w}{\partial y} & 1 + \frac{\partial w}{\partial z} \end{bmatrix}. \quad (10)$$

Finally, we can get the deformation gradient from the reference state  $\mathbf{B}_r$  to the wrinkled state  $\mathbf{B}_w$  as  $\mathbf{F} = \mathbf{F}_1 \cdot \mathbf{F}_0$ . With the help of the deformation gradient  $\mathbf{F}$ , we can obtain the left Cauchy-Green strain tensor  $\mathbf{B} = \mathbf{F} \cdot \mathbf{F}^T$ .

Based on the assumption of the ideal DE model, Cauchy stress in the DE sheet can be decomposed into elastic stress and Maxwell stress

$$\boldsymbol{\sigma} = \boldsymbol{\sigma}_e + \boldsymbol{\sigma}_m, \quad (11)$$

where the elastic stress  $\boldsymbol{\sigma}_e$  can be described by strain energy density  $W_s$  of the incompressible elastomer. The stress  $\boldsymbol{\sigma}_e = \mathbf{F}(\partial W_s / \partial \mathbf{F}) - p\mathbf{I}$  can be described by the deformation gradient  $\mathbf{F}$  and hydrostatic pressure  $p$  as well as unit matrix  $\mathbf{I}$ . In this paper, the neo-Hookean model [33] is adopted. One can obtain

$$\boldsymbol{\sigma}_e = \mu\mathbf{B} - p\mathbf{I}, \quad (12)$$

and the Maxwell stress is a diagonal tensor

$$\boldsymbol{\sigma}_m = \text{diag}\left(-\frac{1}{2}\varepsilon E^2, -\frac{1}{2}\varepsilon E^2, \frac{1}{2}\varepsilon E^2\right). \quad (13)$$

Here, considering the incompressibility of the DE material, we can get

$$\frac{\partial u}{\partial x} + \frac{\partial v}{\partial y} + \frac{\partial w}{\partial z} = 0. \quad (14)$$

And substituting Eqs. (12) and (13) into Eq. (11), we can obtain

$$\begin{aligned}\frac{\partial u}{\partial x} &= \frac{1}{2\mu\lambda_x^2} \left( \sigma_{xx} + p + \frac{\varepsilon E^2}{2} \right) - \frac{1}{2}, \\ \frac{\partial v}{\partial y} &= \frac{1}{2\mu\lambda_y^2} \left( \sigma_{yy} + p + \frac{\varepsilon E^2}{2} \right) - \frac{1}{2}, \\ \frac{\partial w}{\partial z} &= \frac{1}{2\mu\lambda_z^2} \left( \sigma_{zz} + p + \frac{\varepsilon E^2}{2} \right) - \frac{1}{2}.\end{aligned}\quad (15)$$

Combining Eqs. (14) and (15), we can get

$$p = \frac{3\mu\lambda_x^2\lambda_y^2 - \lambda_y^2\sigma_{xx} - \lambda_x^2\sigma_{yy} - \lambda_x^4\lambda_y^4\sigma_{zz} + \lambda_x^4\lambda_y^4\varepsilon E^2}{\lambda_x^2 + \lambda_y^2 + \lambda_x^4\lambda_y^4} - \frac{\varepsilon E^2}{2}. \quad (16)$$

Substituting Eq. (16) back into Eq. (11), we can get the specific expressions of the constitutive equation. Hereon, according to the traditional plate theory [34], the stress components in the  $z$  direction can be ignored. In addition, we can also derive the displacement relationships of  $u = -z\frac{\partial w}{\partial x}$ ,  $v = -z\frac{\partial w}{\partial y}$ . Therefore, we can further obtain the nonzero stress components with a distance  $z$  from the middle plane of DE sheet as follows:

$$\begin{aligned}\begin{Bmatrix} \sigma_{xx} \\ \sigma_{yy} \\ \sigma_{xy} \end{Bmatrix} &= \begin{Bmatrix} \mu(\lambda_x^2 - \lambda_x^{-2}\lambda_y^{-2}) - \varepsilon E^2 \\ \mu(\lambda_y^2 - \lambda_x^{-2}\lambda_y^{-2}) - \varepsilon E^2 \\ 0 \end{Bmatrix} \\ &- z \begin{bmatrix} C_{11} & C_{12} & 0 \\ C_{21} & C_{22} & 0 \\ 0 & 0 & C_{33} \end{bmatrix} \begin{Bmatrix} \frac{\partial^2 w}{\partial x^2} \\ \frac{\partial^2 w}{\partial y^2} \\ \frac{\partial^2 w}{\partial x \partial y} \end{Bmatrix},\end{aligned}\quad (17)$$

where  $C_{11} = 2\mu(\lambda_x^2 + \lambda_x^{-2}\lambda_y^{-2})$ ,  $C_{22} = 2\mu(\lambda_y^2 + \lambda_x^{-2}\lambda_y^{-2})$ ,  $C_{12} = C_{21} = 2\mu\lambda_x^{-2}\lambda_y^{-2}$  and  $C_{33} = \mu(\lambda_x^2 + \lambda_y^2)$ . Then, we can

obtain the bending moments  $M_{xx}$ ,  $M_{yy}$  and twisting moment  $M_{xy}$  through the following integral formula:

$$\begin{Bmatrix} M_{xx} \\ M_{yy} \\ M_{xy} \end{Bmatrix} = \int_{-h/2}^{h/2} \begin{Bmatrix} \sigma_{xx} \\ \sigma_{yy} \\ \sigma_{xy} \end{Bmatrix} z dz. \quad (18)$$

According to the plate theory, the force balance condition in the normal direction requires that

$$\begin{aligned} \frac{\partial^2 M_{xx}}{\partial x^2} + 2 \frac{\partial^2 M_{xy}}{\partial x \partial y} + \frac{\partial^2 M_{yy}}{\partial y^2} + N_{xx} \frac{\partial^2 w}{\partial x^2} \\ + 2N_{xy} \frac{\partial^2 w}{\partial x \partial y} + N_{yy} \frac{\partial^2 w}{\partial y^2} = 0, \end{aligned} \quad (19)$$

where  $N_{xx} = \int_{-h/2}^{h/2} \sigma_{xx} dz$ ,  $N_{yy} = \int_{-h/2}^{h/2} \sigma_{yy} dz$  and  $N_{xy} = \int_{-h/2}^{h/2} \sigma_{xy} dz$  are all the membrane forces.

According to the geometry model of DE sheet in Fig. 1, we can obtain the following boundary conditions and continuity conditions

$$\begin{aligned} w|_{x=0} = 0, \quad \left. \frac{\partial w}{\partial x} \right|_{x=0} = 0, \\ w|_{x=l} = 0, \quad \left. \frac{\partial w}{\partial x} \right|_{x=l} = 0, \end{aligned} \quad (20)$$

and

$$w^-|_{x=a} = w^+|_{x=a}, \quad \left. \frac{\partial w^-}{\partial x} \right|_{x=a} = \left. \frac{\partial w^+}{\partial x} \right|_{x=a}. \quad (21)$$

On left and right sides of the position  $x = a$  in Fig. 1(c), the bending moments are equal and the vertical shear forces are also equal, namely

$$M_{xx}^-|_{x=a} = M_{xx}^+|_{x=a}, \quad Q_x^-|_{x=a} = Q_x^+|_{x=a}, \quad (22)$$

where  $Q_x = \frac{\partial M_{xx}}{\partial x} + 2 \frac{\partial M_{xy}}{\partial y}$  is the so-called effective shear force, which has considered the shear force balance caused by the twisting moment  $M_{xy}$ .

A combination of Eq. (19) with conditions of Eqs. (20)–(22) sets an eigenvalue problem. The deflection of DE sheet can be assumed as following function:

$$w = f(x) \cos(ky), \quad (23)$$

where  $f(x)$  is a single variable function, and  $k$  is wave number of wrinkle.

Substituting Eq. (23) into Eq. (19), we can obtain the following homogeneous ordinary differential equation

$$D_1 \frac{d^4 f(x)}{dx^4} + D_2 \frac{d^2 f(x)}{dx^2} + D_3 f(x) = 0, \quad (24)$$

where, for the zone of  $0 \leq x \leq a$

$$\begin{aligned} D_1 &= -\frac{H^3 \mu (\lambda_{xL}^4 \lambda_y^2 + 1)}{6\lambda_{xL}^5 \lambda_y^5}, \\ D_2 &= -\frac{\varepsilon \Phi^2 \lambda_{xL} \lambda_y}{H} + \frac{H \mu (\lambda_{xL}^4 \lambda_y^2 - 1)}{\lambda_{xL}^3 \lambda_y^3} \\ &\quad + \frac{k^2 H^3 \mu (\lambda_{xL}^4 \lambda_y^2 + \lambda_{xL}^2 \lambda_y^4 + 2)}{6\lambda_{xL}^5 \lambda_y^5}, \end{aligned}$$

$$\begin{aligned} D_3 &= \frac{k^2 \varepsilon \Phi^2 \lambda_{xL} \lambda_y}{H} - \frac{k^2 H \mu (\lambda_{xL}^2 \lambda_y^4 - 1)}{\lambda_{xL}^3 \lambda_y^3} \\ &\quad - \frac{k^4 H^3 \mu (\lambda_{xL}^2 \lambda_y^4 + 1)}{6\lambda_{xL}^5 \lambda_y^5}, \end{aligned} \quad (25a)$$

and for the zone of  $a \leq x \leq l$

$$\begin{aligned} D_1 &= -\frac{H^3 \mu (\lambda_{xR}^4 \lambda_y^2 + 1)}{6\lambda_{xR}^5 \lambda_y^5}, \\ D_2 &= \frac{H \mu (\lambda_{xR}^4 \lambda_y^2 - 1)}{\lambda_{xR}^3 \lambda_y^3} + \frac{k^2 H^3 \mu (\lambda_{xR}^4 \lambda_y^2 + \lambda_{xR}^2 \lambda_y^4 + 2)}{6\lambda_{xR}^5 \lambda_y^5}, \\ D_3 &= -\frac{k^2 H \mu (\lambda_{xR}^2 \lambda_y^4 - 1)}{\lambda_{xR}^3 \lambda_y^3} - \frac{k^4 H^3 \mu (\lambda_{xR}^2 \lambda_y^4 + 1)}{6\lambda_{xR}^5 \lambda_y^5}. \end{aligned} \quad (25b)$$

In Eq. (24), we will define the dimensionless quantities: dimensionless coordinate  $\bar{x} = x/H$ , dimensionless width  $\bar{a} = a/H$  and  $\bar{l} = l/H$ , dimensionless thickness  $\bar{h} = h/H$ , dimensionless stresses  $\bar{\sigma}_{xx} = \sigma_{xx}/\mu$  and  $\bar{\sigma}_{yy} = \sigma_{yy}/\mu$ , dimensionless voltage  $\bar{\Phi} = \Phi/(H\sqrt{\mu/\varepsilon})$ , and dimensionless wave number  $\bar{k} = kH$ . The dimensionless coefficients are given as follows: for the zone of  $0 \leq \bar{x} \leq \bar{a}$

$$\begin{aligned} \bar{D}_1 &= -\frac{\lambda_{xL}^4 \lambda_y^2 + 1}{6\lambda_{xL}^5 \lambda_y^5}, \\ \bar{D}_2 &= -\bar{\Phi}^2 \lambda_{xL} \lambda_y + \frac{\lambda_{xL}^4 \lambda_y^2 - 1}{\lambda_{xL}^3 \lambda_y^3} + \frac{\bar{k} (\lambda_{xL}^4 \lambda_y^2 + \lambda_{xL}^2 \lambda_y^4 + 2)}{6\lambda_{xL}^5 \lambda_y^5}, \\ \bar{D}_3 &= \bar{k}^2 \bar{\Phi}^2 \lambda_{xL} \lambda_y - \frac{\bar{k}^2 (\lambda_{xL}^2 \lambda_y^4 - 1)}{\lambda_{xL}^3 \lambda_y^3} - \frac{\bar{k}^4 (\lambda_{xL}^2 \lambda_y^4 + 1)}{6\lambda_{xL}^5 \lambda_y^5}, \end{aligned} \quad (26a)$$

for the zone of  $\bar{a} \leq \bar{x} \leq \bar{l}$

$$\begin{aligned} \bar{D}_1 &= -\frac{\lambda_{xR}^4 \lambda_y^2 + 1}{6\lambda_{xR}^5 \lambda_y^5}, \\ \bar{D}_2 &= \frac{\lambda_{xR}^4 \lambda_y^2 - 1}{\lambda_{xR}^3 \lambda_y^3} + \frac{\bar{k} (\lambda_{xR}^4 \lambda_y^2 + \lambda_{xR}^2 \lambda_y^4 + 2)}{6\lambda_{xR}^5 \lambda_y^5}, \\ \bar{D}_3 &= -\frac{\bar{k}^2 (\lambda_{xR}^2 \lambda_y^4 - 1)}{\lambda_{xR}^3 \lambda_y^3} - \frac{\bar{k}^4 (\lambda_{xR}^2 \lambda_y^4 + 1)}{6\lambda_{xR}^5 \lambda_y^5}. \end{aligned} \quad (26b)$$

Substituting Eq. (23) into Eqs. (20) and (21), we can very easily get the corresponding dimensionless expressions of the boundary conditions and continuity conditions. So we will not elaborate here. However, the bending moment and shear force balance conditions in Eq. (22) will be given explicitly as follows:

$$\begin{aligned} \frac{(1 + \lambda_{xL}^4 \lambda_{y0}^2) \frac{d^2 \bar{f}}{d\bar{x}^2} - \bar{k}^2 \bar{f}}{\lambda_{xL}^5} &= \frac{(1 + \lambda_{xR}^4 \lambda_{y0}^2) \frac{d^2 \bar{f}}{d\bar{x}^2} - \bar{k}^2 \bar{f}}{\lambda_{xR}^5}, \quad (27) \\ \frac{\bar{k}^2 (1 + \lambda_{xL}^4 \lambda_{y0}^2 + \lambda_{xL}^2 \lambda_{y0}^4) \frac{d\bar{f}}{d\bar{x}} - (1 + \lambda_{xL}^4 \lambda_{y0}^2) \frac{d^3 \bar{f}}{d\bar{x}^3}}{\lambda_{xL}^5} &= \frac{\bar{k}^2 (1 + \lambda_{xR}^4 \lambda_{y0}^2 + \lambda_{xR}^2 \lambda_{y0}^4) \frac{d\bar{f}}{d\bar{x}} - (1 + \lambda_{xR}^4 \lambda_{y0}^2) \frac{d^3 \bar{f}}{d\bar{x}^3}}{\lambda_{xR}^5}. \end{aligned} \quad (28)$$



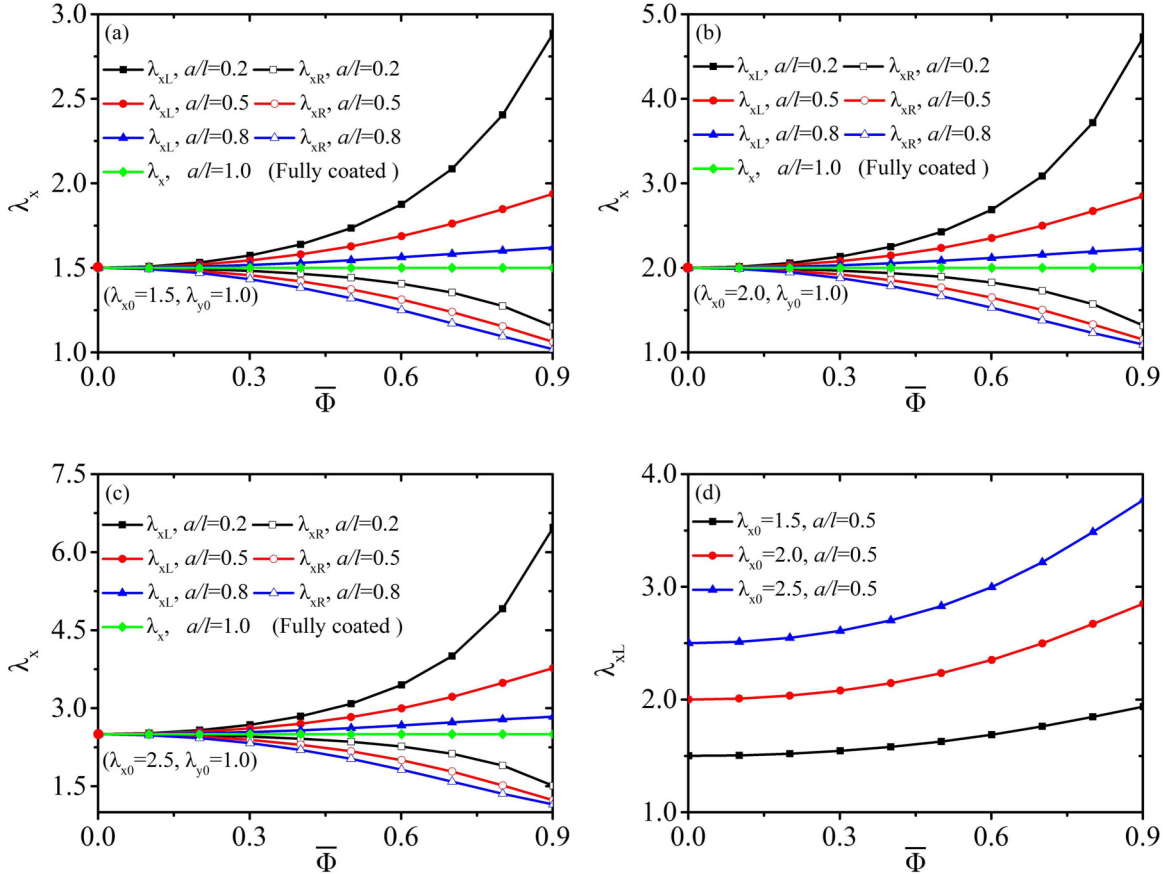


FIG. 2. The effect of the applied voltage on the stretches  $\lambda_{xL}$  and  $\lambda_{xR}$  for the different width ratios of striped electrodes: (a)  $\lambda_{x0} = 1.5$ , (b)  $\lambda_{x0} = 2.0$ , and (c)  $\lambda_{x0} = 2.5$ . (d) The effect of the applied voltage on the stretch  $\lambda_{xL}$  for the width ratio  $a/l = 0.5$ . With the increase of applied voltage, the stretch  $\lambda_{xL}$  increases, while  $\lambda_{xR}$  decreases. Under the conditions of the same applied voltage and width ratio  $a/l = 0.5$ , the stretch  $\lambda_{xL}$  increases with the increase of prestretch.

After the governing Eq. (24) being dimensionless, only width ratio  $a/l$  is the system parameter that can be adjusted in the theoretical analysis. The membrane stresses  $\bar{\sigma}_{xx}^L$  and  $\bar{\sigma}_{yy}^L$  as well as the stretches  $\lambda_{xL}$  and  $\lambda_{xR}$  are all dependent on the electric field intensity  $\bar{E}$  caused by voltage  $\bar{\Phi}$ . For a given  $a/l$ , the eigenvalue of voltage in Eq. (24) can be solved numerically by virtue of the function of *bvp5c* in *Matlab* and the corresponding eigenvector is the waveform of wrinkling.

### III. RESULTS AND DISCUSSIONS

A nonlinear plate theory is introduced to investigate the wrinkling phenomenon of a DE sheet subjected to electromechanical loading. In the following, we calculate the membrane stresses by using Eq. (6), and obtain the critical voltages and wrinkling mode of DE sheet by solving Eq. (24).

#### A. Prebuckling stress field in the DE sheet

In order to obtain the prebuckling stress state in the DE sheet, the principal stretches  $\lambda_{xL}$  and  $\lambda_{xR}$  in Eq. (7) will be solved first with the boundary condition of Eq. (8) by using the software of Mathematica. It should be mentioned here that the principal stretches  $\lambda_{xL}$  and  $\lambda_{xR}$  depend on the applied voltage  $\bar{\Phi}$ . Subsequently, substituting the stretches into Eq. (6), the stresses  $\bar{\sigma}_{xx}^L$ ,  $\bar{\sigma}_{xx}^R$ ,  $\bar{\sigma}_{yy}^L$ , and  $\bar{\sigma}_{yy}^R$  can be easily obtained and

they are also dependent on the applied voltage  $\bar{\Phi}$ . Figure 2 plots the effect of the applied voltage on the stretches  $\lambda_{xL}$  and  $\lambda_{xR}$  for the different width ratios of striped electrodes ( $a/l = 0.2, 0.5, 0.8, \text{ and } 1.0$ ). With the increase of applied voltage, the stretch  $\lambda_{xL}$  increases, while  $\lambda_{xR}$  decreases as shown in Figs. 2(a)–2(c). In other words, for all the width ratios, the current area of electrode always increases with the increase of the applied voltage. This is because the larger the applied voltage, the larger the Maxwell stress. It is worth noting that  $a/l = 1.0$  means that the DE sheet is fully coated with electrodes, and thus  $\lambda_x = \lambda_{x0}$ . In addition, in order to study the influence of prestretch on the deformation, the stretch  $\lambda_{xL}$  is taken as an example as shown in Fig. 2(d). It can be seen that under the conditions of the same applied voltage and width ratio, the stretch  $\lambda_{xL}$  increases with the increase of prestretch. This indicates that the prestretch can effectively affect the deformation of DE sheet.

After the functions of  $\lambda_{xL}$  and  $\lambda_{xR}$  about the applied voltage having been obtained, we can substitute the above functions into Eq. (6) to get the stresses  $\bar{\sigma}_{xx}^L$ ,  $\bar{\sigma}_{xx}^R$ ,  $\bar{\sigma}_{yy}^L$  and  $\bar{\sigma}_{yy}^R$ . Figure 3 plots the effect of the applied voltage on the stresses  $\bar{\sigma}_{xx}^L$  and  $\bar{\sigma}_{xx}^R$  for the different width ratios ( $a/l = 0.2, 0.5, 0.8, \text{ and } 1.0$ ). Generally, the stresses  $\bar{\sigma}_{xx}^L$  and  $\bar{\sigma}_{xx}^R$  both decrease with the increase of applied voltage as shown in Figs. 3(a)–3(c). However, the stress  $\bar{\sigma}_{xx}^L$  with the width ratio  $a/l = 0.2$

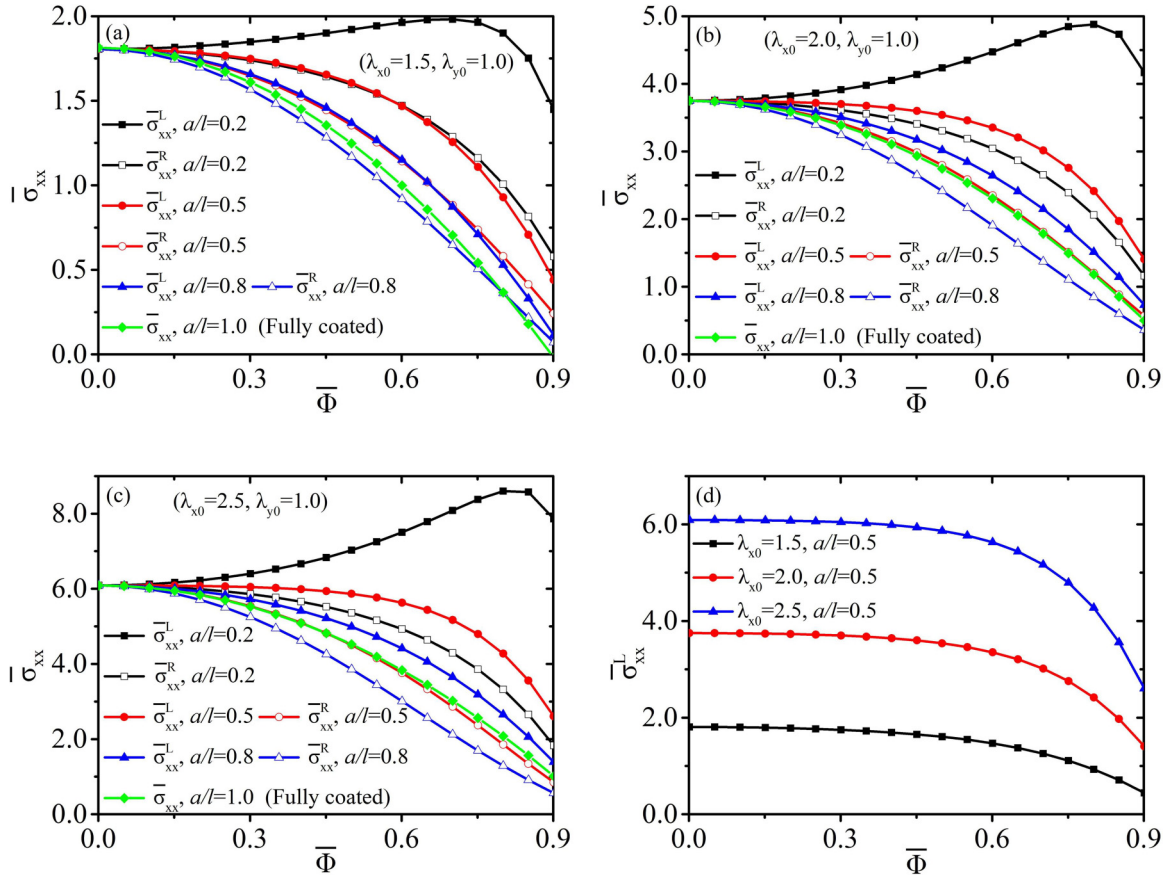


FIG. 3. The effect of the applied voltage on the stresses  $\bar{\sigma}_{xx}^L$  and  $\bar{\sigma}_{xx}^R$  for the different width ratios of striped electrodes. (a)  $\lambda_{x0} = 1.5$ , (b)  $\lambda_{x0} = 2.0$ , and (c)  $\lambda_{x0} = 2.5$ . (d) The effect of the applied voltage on the stress  $\bar{\sigma}_{xx}^L$  for the width ratio  $a/l = 0.5$ . Generally, the stresses  $\bar{\sigma}_{xx}^L$  and  $\bar{\sigma}_{xx}^R$  both decrease with the increase of applied voltage. However, the  $\bar{\sigma}_{xx}^L$  with  $a/l = 0.2$  appears to increase first and then decrease. Under the conditions of the same applied voltage and width ratio  $a/l = 0.5$ , the stress  $\bar{\sigma}_{xx}^L$  increases with the increase of prestretch.

appears to increase first and then decrease. The reason for this phenomenon is that the thickness of electrode zone  $a/l = 0.2$  becomes thinner sharply as shown by the black square-line in Fig. 4(a). In this case, the total stress is determined by the competition between the elastic stress and Maxwell stress

as shown in Fig. 4(b). With the increase of applied voltage, the total stress  $\bar{\sigma}_{xx}^L$  appears to increase when the elastic stress increment is dominant, but decreases when the Maxwell stress increment is dominant. For  $a/l = 0.5, 0.8$ , and  $1.0$ , the Maxwell stress increment is dominant with the increase of

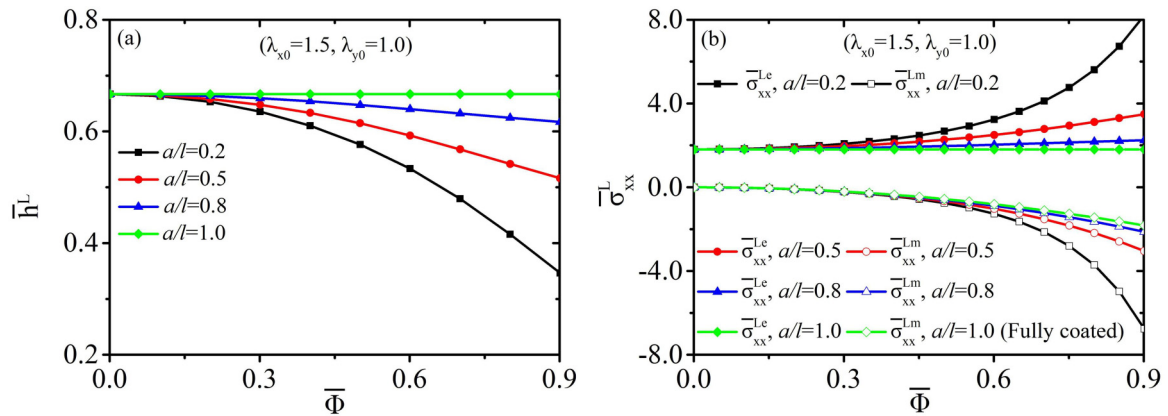


FIG. 4. The effect of the applied voltage on the thickness  $\bar{h}^L$  and stress  $\bar{\sigma}_{xx}^L$  for the different width ratios of striped electrodes. (a) The current thickness  $\bar{h}^L$  of the left part of DE sheet; (b) the elastic stress  $\bar{\sigma}_{xx}^{Le}$  and Maxwell stress  $\bar{\sigma}_{xx}^{Lm}$ . The thickness for electrode zone  $a/l = 0.2$  becomes thinner sharply than that for the other electrode zones  $a/l = 0.5, 0.8$ , and  $1.0$ . With the increase of applied voltage, the elastic stress  $\bar{\sigma}_{xx}^{Le}$  increases while Maxwell stress  $\bar{\sigma}_{xx}^{Lm}$  decreases. The total stress  $\bar{\sigma}_{xx}^L$  is determined by the competition between the elastic stress and Maxwell stress, which causes the  $\bar{\sigma}_{xx}^L$  with  $a/l = 0.2$  to increase first and then decrease as shown in Fig. 3(a).

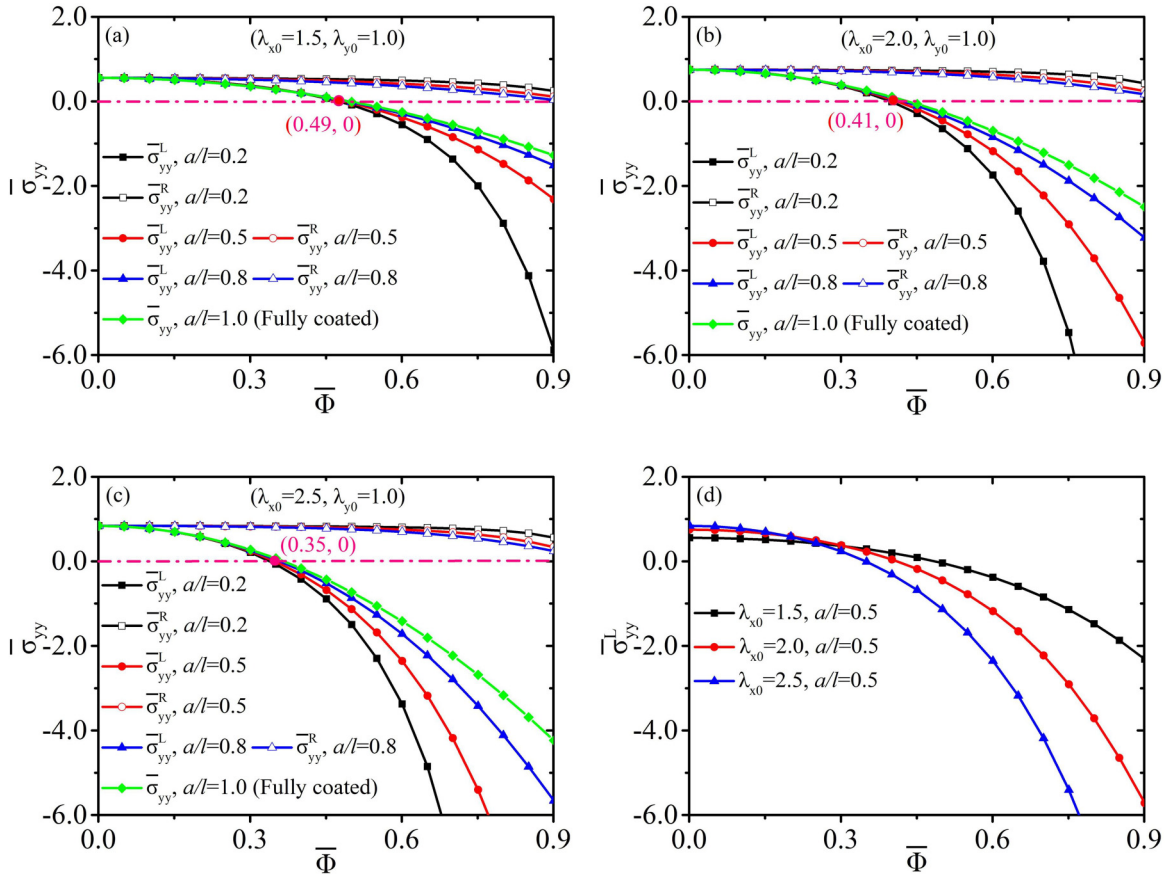


FIG. 5. The effect of the applied voltage on the stresses  $\bar{\sigma}_{yy}^L$  and  $\bar{\sigma}_{yy}^R$  for the different width ratio of striped electrodes. (a)  $\lambda_{x0} = 1.5$ , (b)  $\lambda_{x0} = 2.0$ , and (c)  $\lambda_{x0} = 2.5$ . (d) The effect of the applied voltage on the stress  $\bar{\sigma}_{yy}^L$  for the width ratio  $a/l = 0.5$ . The stresses  $\bar{\sigma}_{yy}^L$  and  $\bar{\sigma}_{yy}^R$  both decrease with the increase of applied voltage. And the stress  $\bar{\sigma}_{yy}^L$  in the electrode zone changes quickly from tensile stress to compressive stress. This is the cause of wrinkling.

applied voltages as shown by the red circle-line, blue triangle-line, and green rhombus-line in Fig. 4(b). In order to study the influence of prestretch on the stress, the stress  $\bar{\sigma}_{xx}^L$  with the width ratio  $a/l = 0.5$  is taken as an example as shown in Fig. 3(d). It can be seen that under the conditions of the same applied voltage and width ratio, the stress  $\bar{\sigma}_{xx}^L$  increases with the increase of prestretch. This indicates that the prestretch can effectively change stress distribution in the DE sheet.

Figure 5 plots the effect of the applied voltage on the stresses  $\bar{\sigma}_{yy}^L$  and  $\bar{\sigma}_{yy}^R$  for the different width ratios ( $a/l = 0.2, 0.5, 0.8$ , and  $1.0$ ). It can be seen from Fig. 5 that the stresses  $\bar{\sigma}_{yy}^L$  and  $\bar{\sigma}_{yy}^R$  both decrease with the increase of applied voltage. And the stress  $\bar{\sigma}_{yy}^L$  in the electrode zone changes quickly from tensile stress to compressive stress as shown in Figs. 5(a)–5(c), while the stress  $\bar{\sigma}_{yy}^R$  in the nonelectrode zone is tensile stress. It also should be mentioned here that the compressive stress  $\bar{\sigma}_{yy}^L$  is the reason of voltage induced wrinkling. With the increase of prestretch, the required voltage for the onset of compressive stress decreases gradually (i.e., 0.49, 0.41 and 0.35 as shown in Figs. 5(a)–5(c)). These three voltages are the critical voltages obtained from the criterion of loss of tension. The stress  $\bar{\sigma}_{yy}^L$  with the width ratio  $a/l = 0.5$  is taken as an example to study the influence of prestretch on the stress as shown in Fig. 5(d). It can be

seen from Fig. 5(d) that under the conditions of the same applied voltage and width ratio  $a/l = 0.5$ , the compressive stresses increase with the increase of prestretch at the applied voltage larger than 0.3. This can be understood by the rewritten stresses  $\sigma_{xx}^L = \lambda_{xL}^2(\mu - \varepsilon\lambda_y^2(\frac{\Phi}{H})^2) - \mu\lambda_{xL}^{-2}\lambda_y^{-2}$  and  $\sigma_{yy}^L = \mu(\lambda_y^2 - \lambda_{xL}^{-2}\lambda_y^{-2}) - \varepsilon\lambda_{xL}^2\lambda_y^2(\frac{\Phi}{H})^2$  obtained by substituting the equations  $\lambda_{zL} = 1/\lambda_{xL}\lambda_y$ ,  $h^L = H\lambda_{zL}$ , and  $E = \Phi/h^L$  into Eqs. 6(a) and 6(b). Obviously, the stress  $\sigma_{xx}^L$  increases with the increase of prestretch  $\lambda_{xL}$  when the other parameters keep constant, while  $\sigma_{yy}^L$  is determined by the competition between the elastic stress  $\mu(\lambda_y^2 - \lambda_{xL}^{-2}\lambda_y^{-2})$  and Maxwell stress  $-\varepsilon\lambda_{xL}^2\lambda_y^2(\frac{\Phi}{H})^2$ . With the increase of prestretch  $\lambda_{xL}$ , the elastic stress increases while Maxwell stress decreases when the other parameters keep constant. Therefore, with the increase of prestretch, the stresses may increase in both directions at voltages lower than 0.3. In this case, the compressive stresses in the y-axis direction can be augmented by increasing prestretch to promote wrinkling of the DE sheet.

Figure 6 plots the effect of the applied voltage on the stresses  $\bar{\sigma}_{xx}$  and  $\bar{\sigma}_{yy}$  for the different prestretches ( $\lambda_{y0} = 1.0, 1.5$ , and  $2.0$ ). It can be seen from Fig. 6 that both the stress  $\bar{\sigma}_{xx}$  and stress  $\bar{\sigma}_{yy}$  decrease with the increase of applied voltage. With the increase of prestretch, the variation of stress with applied voltage becomes steeper. For the width ratio

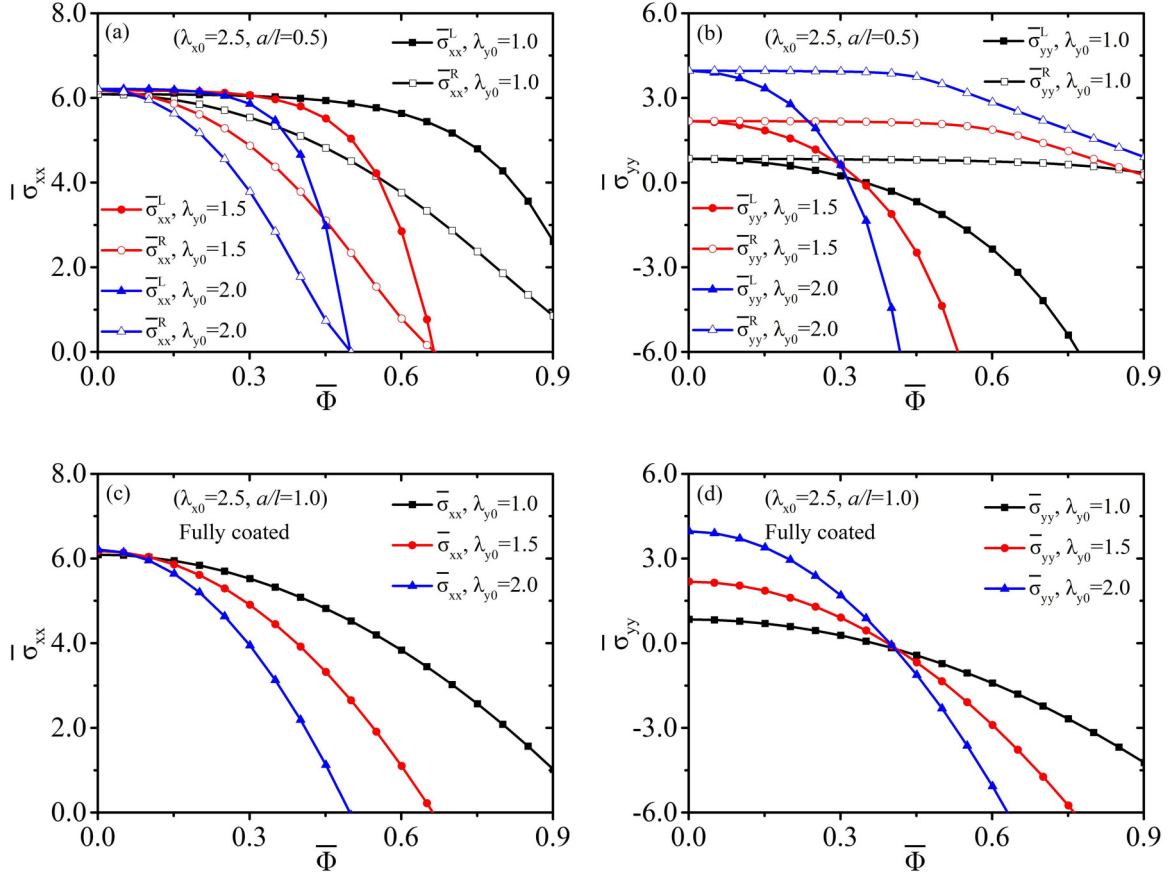


FIG. 6. The effect of the applied voltage on the stresses  $\bar{\sigma}_{xx}$  and  $\bar{\sigma}_{yy}$  with the different prestretches. (a)  $\bar{\sigma}_{xx}$  for  $a/l = 0.5$ , (b)  $\bar{\sigma}_{yy}$  for  $a/l = 0.5$ , (c)  $\bar{\sigma}_{xx}$  for  $a/l = 1.0$ , and (d)  $\bar{\sigma}_{yy}$  for  $a/l = 1.0$ . For a given width ratio  $a/l$ , both the stress  $\bar{\sigma}_{xx}$  and stress  $\bar{\sigma}_{yy}$  decrease with the increase of applied voltage. With the increase of prestretch  $\lambda_{y0}$ , the variation of stresses  $\bar{\sigma}_{xx}$  and  $\bar{\sigma}_{yy}$  with applied voltage becomes steeper.

$a/l = 0.5$ , the stress  $\bar{\sigma}_{xx}^L$  in the electrode zone and the stress  $\bar{\sigma}_{xx}^R$  in the nonelectrode zone intersect at zero as shown in Fig. 6(a). This is because the forces between the left part and right part of DE sheet are balanced in the  $x$ -axis direction. When  $\bar{\sigma}_{xx}^L$  is equal to zero,  $\bar{\sigma}_{xx}^R$  must be equal to zero. For large applied voltages, the compressive stress  $\bar{\sigma}_{yy}^L$  increases with the increase of prestretch  $\lambda_{y0}$  as shown in Fig. 6(b). This means that the larger the prestretch  $\lambda_{y0}$  is, the more likely it is to cause wrinkling instability of DE sheet. There are some similar results existing in DE sheets with fully coated electrodes ( $a/l = 1.0$ ) as shown in Figs. 6(c) and 6(d).

### B. Critical condition for the voltage-driven wrinkling

Wrinkling phenomenon is an important electromechanical failure mode of a DE sheet. According to the analysis of the stress state in Sec. III A, when the applied voltage  $\bar{\Phi}$  increases to a certain value, the compressive stress in the DE sheet may appear. And when the compressive stress is larger than a critical value, the wrinkles of DE sheet will appear. Depending on magnitude of applied voltage, the DE sheet may stay in one of the two phases: flat and wrinkling. For a given  $a/l$  and  $\bar{k}$ , the critical voltage  $\bar{\Phi}_c$  for the onset of wrinkles can be calculated by solving the eigenvalue of the governing Eq. (24). In the following, we investigate the effect of the width ratio

of striped electrode and prestretch on the critical voltage and wavelength.

Figure 7 plots the dependence of the critical voltage  $\bar{\Phi}_c$  on wave numbers for three kinds of prestretches ( $\lambda_{x0} = 1.5, 2.0, \text{ and } 2.5$ ). For a given  $a/l$ , there exists a minimum critical voltage  $\bar{\Phi}_{th}$  at a certain  $\bar{k}_{th}$ , in which  $\bar{\Phi}_{th}$  and  $\bar{k}_{th}$  are named as threshold voltage and the most easily wrinkling wave number, respectively. In other words, only when the voltage reaches the threshold voltage, will the DE sheet wrinkle at a certain wavelength. The critical wavelength of wrinkling results from the competition between the bending energy and stretching energy [28]. With the increase of wave number, the critical voltage  $\bar{\Phi}_c$  decreases first and then increases as shown in Figs. 7(a)–7(c). For a given prestretch, the minimum threshold voltage (or named as optimal threshold voltage)  $\bar{\Phi}_{th}^{opt}$  appears and corresponds to the optimal width ratio  $\bar{w}_r^{opt} = a/l$  and wave number  $\bar{k}_{th}^{opt}$ . For the prestretch  $\lambda_{x0} = 1.5$ , the optimal width ratio  $\bar{w}_r^{opt} = 0.4$ , optimal wave number  $\bar{k}_{th}^{opt} = 0.6$ , and optimal threshold voltage  $\bar{\Phi}_{th}^{opt} = 0.5019$  as shown in Fig. 7(a). For the prestretch  $\lambda_{x0} = 2.0$ ,  $\bar{w}_r^{opt} = 0.3$ ,  $\bar{k}_{th}^{opt} = 1.0$  and  $\bar{\Phi}_{th}^{opt} = 0.4196$  as shown in Fig. 7(b). For the prestretch  $\lambda_{x0} = 2.5$ ,  $\bar{w}_r^{opt} = 0.3$ ,  $\bar{k}_{th}^{opt} = 1.3$ , and  $\bar{\Phi}_{th}^{opt} = 0.3568$  as shown in Fig. 7(c). It is worth mentioning that there exists an optimal width ratio in each case of prestretches of  $\lambda_{x0} = 1.5, 2.0, 2.5$ . Hereon, we take the prestretch  $\lambda_{x0} = 1.5$  as



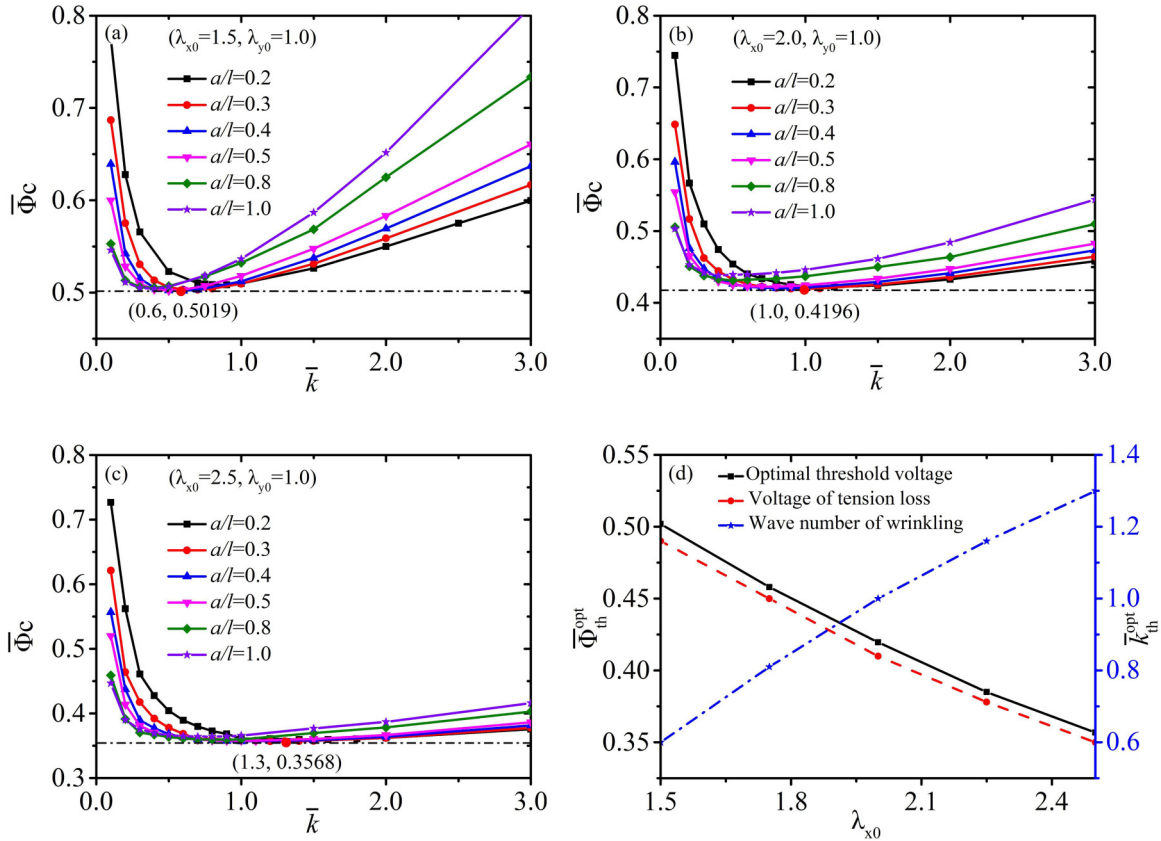


FIG. 7. The influences of prestretches on critical voltage and wave number for different width ratio of striped electrodes. (a)  $\lambda_{x0} = 1.5$ , (b)  $\lambda_{x0} = 2.0$ , and (c)  $\lambda_{x0} = 2.5$ . (d) The dependence of the optimal threshold voltage and wave number of wrinkling on the prestretch.

an example to investigate the effect of width ratio  $a/l$  on the threshold voltage  $\bar{\Phi}_{th}$ . According to the data drawn in Fig. 7(a), we can get  $\bar{\Phi}_{th} = 0.5084, 0.5030, 0.5019, 0.5021, 0.5043$ , and  $0.5052$  for  $a/l = 0.2, 0.3, 0.4, 0.5, 0.8$ , and  $1.0$ , respectively. It can be seen that the optimal width ratio and optimal threshold voltage are  $\bar{w}_r^{opt} = a/l = 0.4$  and  $\bar{\Phi}_{th}^{opt} = \bar{\Phi}_{th} = 0.5019$ , respectively. With the increase of  $a/l$ , the threshold voltage decreases first and then increases. In engineering applications, it is very challenging to obtain low threshold voltages, and fortunately the optimal width ratio can effectively reduce the threshold voltage.

Based on Figs. 7(a)–7(c), and 7(d) plots the influence of prestretch on the optimal threshold voltage  $\bar{\Phi}_{th}^{opt}$  and wave number  $\bar{k}_{th}^{opt}$ . With the increase of prestretch, the optimal threshold voltages  $\bar{\Phi}_{th}^{opt}$  of wrinkling decrease. This result implies that the prestretch can be tuned to regulate the threshold voltage for different applications. It is noted that the optimal threshold voltages  $\bar{\Phi}_{th}^{opt}$  are all bigger than the corresponding voltages obtained from loss of tension criterion (i.e., for the onset of compressive stress). This results from the fact that the bending energy has a certain inhibiting effect on a wrinkle of the DE sheet. In addition, the wave number  $\bar{k}_{th}^{opt}$  of wrinkling increases with the increase of prestretch. In other words, the corresponding wavelength of wrinkling decreases with the increase of prestretch. This means that the wavelength of wrinkling can be manipulated by controlling prestretch for practical applications.

In addition, in order to study the influence of prestretches in the y-axis direction on the critical voltage and wave number of a DE sheet, a plot with the prestretches  $\lambda_{y0} = 1.0, 1.5$ , and  $2.0$  as well as width ratio  $a/l = 0.5$  is taken as an example as shown in Fig. 8. For  $\lambda_{y0} = 1.0$ , the threshold voltage  $\bar{\Phi}_{th} = 0.3579$  and corresponding wave number  $\bar{k}_{th} = 1.0$ . For  $\lambda_{y0} = 1.5$ ,  $\bar{\Phi}_{th} = 0.3423$ , and  $\bar{k}_{th} = 1.05$ . For  $\lambda_{y0} = 2.0$ ,  $\bar{\Phi}_{th} = 0.3194$ , and  $\bar{k}_{th} = 1.1$ . It can be concluded that the threshold voltage  $\bar{\Phi}_{th}$  of wrinkling decreases with the increase

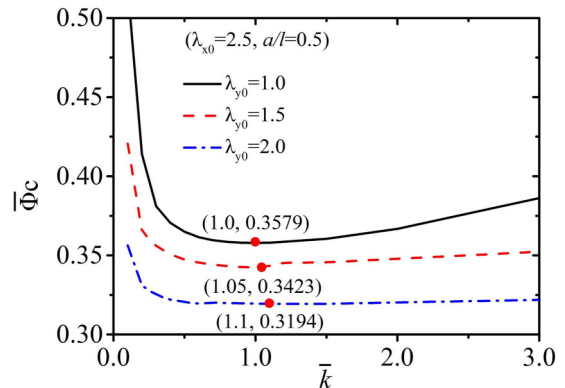


FIG. 8. The dependence of critical voltage on wave number for different prestretches. The threshold voltages  $\bar{\Phi}_{th}$  of wrinkling decrease with the increase of prestretch  $\lambda_{y0}$ .

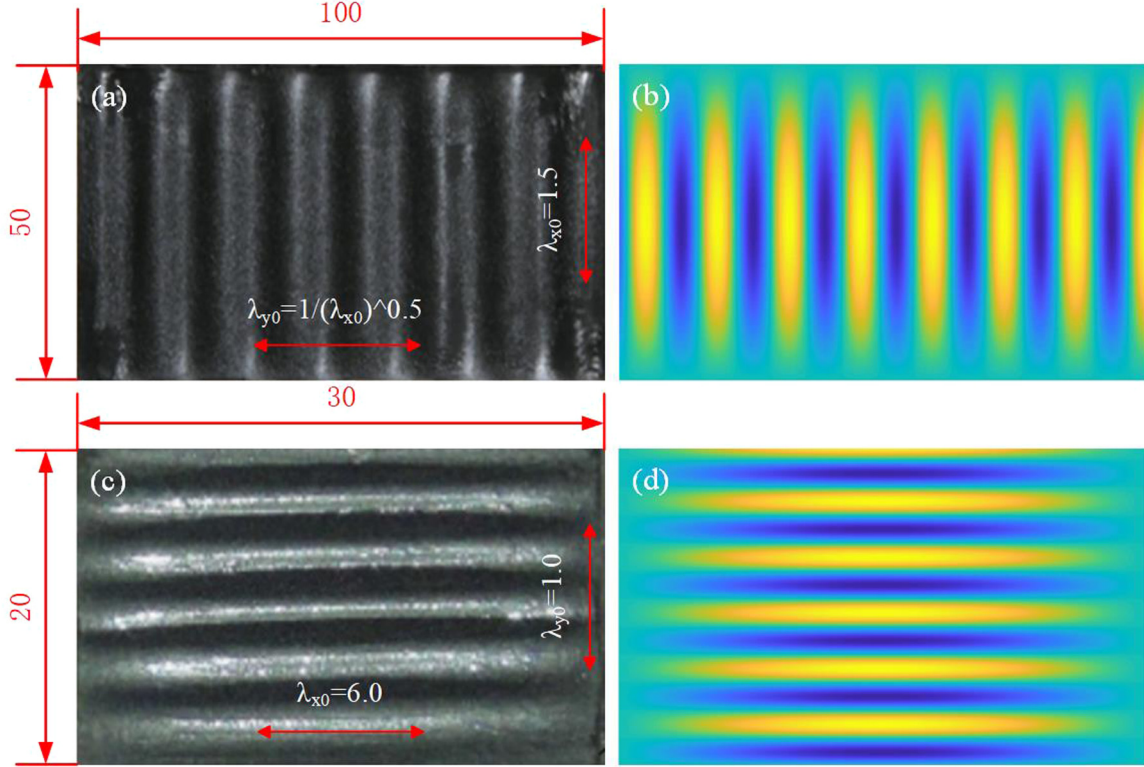


FIG. 9. Comparison of wave forms and wavelengths by theoretical prediction and previous experiments of DE sheet with full coated electrodes: (a) experiment of Ref. [28]; (b) the corresponding theoretical prediction; (c) experiment of Ref. [30] and (d) the corresponding theoretical prediction. The wave form and wavelength of wrinkling obtained from theoretical prediction are in well agreement with the experimental results.

of prestretch  $\lambda_{y0}$ . The reason for this phenomenon is that the compressive stress  $\bar{\sigma}_{yy}^L$  for the large applied voltage increases with the increase of prestretch  $\lambda_{y0}$  as shown in Fig. 6(b). This means that the wrinkling instability can be manipulated by controlling prestretch in the  $y$ -axis direction for practical applications.

### C. Wrinkling mode of the DE sheet

The present model can be used to predict the wrinkling mode of a DE sheet, such as wave form and wavelength of wrinkling. Based on the eigenvector obtained from Eq. (24), Fig. 9 plots the comparison of wave forms and wavelengths by theoretical prediction and previous experiments [28,30] of a DE sheet with full coated electrodes. In the experiments, the wrinkling wave form of a rectangular VHB4905 sheet ( $50 \times 100$  mm) with the prestretches  $\lambda_{x0} = 1.5$  and  $\lambda_{y0} = 1/\sqrt{\lambda_{x0}}$  [28] is shown in Fig. 9(a). And the wrinkling wave form of a rectangular VHB4910 sheet ( $20 \times 30$  mm) with the prestretches  $\lambda_{x0} = 6.0$  and  $\lambda_{y0} = 1.0$  [30] is shown in Fig. 9(c). By setting the same geometry sizes and prestretches as those of the experiments, the corresponding theoretical predictions are given in Figs. 9(b) and 9(d). It can be seen from Fig. 9 that the wave form and wavelength of wrinkling obtained from theoretical prediction are well in agreement with the result of experiment, which indicates the present model is able to provide a good prediction about wrinkling of a DE sheet.

In the experiments [28,30], the top and bottom surfaces of the DE sheet were all coated with carbon grease electrodes.

However, the present model can further predict the mode of DE sheet with different width ratios of a striped electrode. Figure 10 plots the wrinkling mode of the DE sheet with  $a/l = 0.2, 0.5, 0.8,$  and  $1.0$ . In the computation, we take the prestretches  $\lambda_{x0} = 1.5$  and  $\lambda_{y0} = 1.0$  as an example. It can be seen from the figures that the deflection in the electrode area is relatively larger due to wrinkling, while that in nonelectrode area is small because of its tensional state. It is noted that the wavelength corresponding to the wave number of wrinkling increases with the increase of width ratio as shown in Figs. 10(a)–10(d). By controlling the electrode area, various wrinkling patterns can be obtained to meet the functional requirements of luxuriant applications.

Figure 10 also shows the coexistence of wrinkled and flat regions in the dielectric elastomer sheet with striped electrodes, which is different from a DE film with fully coated electrode deformed into the coexistence of thick flat state, as well as thin and large-area wrinkled state due to the constrain of the small-area flat regions [21]. In our work, the DE sheet with width ratio of striped electrodes  $a/l \neq 1.0$  may wrinkle into the coexistence state, in which  $\bar{\sigma}_{yy}^R$  in the nonelectrode zone is tensile while  $\bar{\sigma}_{yy}^L$  triggering the wrinkling in the electrode zone is compressive, caused by the Maxwell stress.

## IV. CONCLUSIONS

Controllable wrinkling of a DE sheet is important for some engineering applications such as diffraction gratings, optical

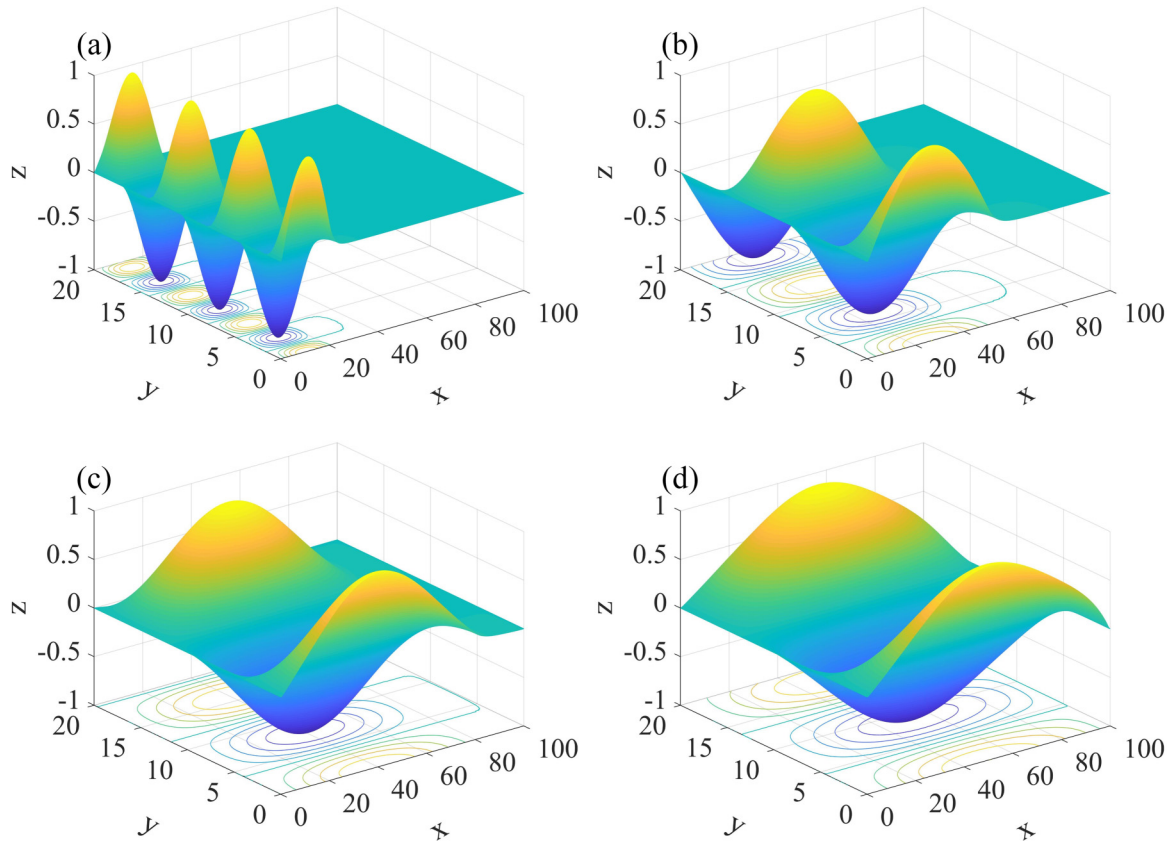


FIG. 10. The wrinkling mode of DE sheet with different width ratios of striped electrode: (a)  $a/l = 0.2$ , (b)  $a/l = 0.5$ , (c)  $a/l = 0.8$ , and (d)  $a/l = 1.0$ . In the computation, we set the prestretches  $\lambda_{x0} = 1.5$  and  $\lambda_{y0} = 1.0$ .

sensors, soft actuators, and adjustable wetting surfaces. To precisely predict and control the threshold voltage and mode of the wrinkling, a large deformation plate theory considering the bending energy and prestretch is used to analyze the wrinkling phenomenon of the DE sheet with striped electrodes. The results show that the prestretch has important influence on the distribution of stress field, threshold voltage, and wavelength of wrinkles. For large applied voltages, with the increase of prestretch, the stress increases in the prestretched direction while decreases in the perpendicular to the prestretched direction, which results in the decreases of the threshold voltage and wavelength of wrinkles. Hereon, the predicted threshold voltage is bigger than the corresponding voltage of the loss of tension, which indicates that the bending energy has a certain inhibiting effect on wrinkling of the DE sheet. In addition, the striped electrodes can also effectively

control the threshold voltage and wavelength. With the increase of width ratio of striped electrodes, the wavelength increases, while the threshold voltage decrease first and then increase. Also, there exists an optimal width ratio of electrode corresponding to the optimal threshold voltage. The results and developed methodology can be used to predict and control the behavior of wrinkling in the engineering applications of DE structures.

#### ACKNOWLEDGMENTS

This research was funded by Natural Science Foundation of Anhui Province (Grant No. 2008085QA50), the Key Project of Natural Science Research of Universities in Anhui (Grants No. KJ2020A0449 and No. KJ2020A0452) and Anhui Sijian Holding Group Co. LTD (Grant No. 2019-K-060).

- 
- [1] J. Huang, T. Li, F. C. Chiang, J. Zhu, D. R. Clarke, and Z. Suo, Giant, voltage-actuated deformation of a dielectric elastomer under dead load, *Appl. Phys. Lett.* **100**, 041911 (2012).
- [2] F. B. Zhu, C. L. Zhang, J. Qian, and W. Q. Chen, Mechanics of dielectric elastomers: Materials, structures, and devices, *J. Zhejiang Univ. Sci. A* **17**, 1 (2016).
- [3] G. Y. Gu, J. Zhu, L. M. Zhu, and X. Zhu, A survey on dielectric elastomer actuators for soft robots, *Bioinspir. Biomim.* **12**, 011003 (2017).
- [4] A. O'Halloran, F. O'Malley, and P. Mchugh, A review on dielectric elastomer actuators, technology, applications, and challenges, *J. Appl. Phys.* **104**, 071101 (2008).
- [5] R. Kornbluh, R. Pelrine, Q. Pei, R. Heydt, S. Stanford, S. Oh, and J. Eckerle, Electroelastomers: Applications of dielectric elastomer transducers for actuation, generation, and smart structures, *Proc. SPIE Int. Soc. Opt. Eng.* **4698**, 254 (2002).
- [6] F. Carpi and D. D. Rossi, Eyeball pseudo-muscular actuators for an android face, *Proc. SPIE Int. Soc. Opt. Eng.* **5759**, 16 (2005).

- [7] Y. Liu, L. Liu, Z. Zhang, Y. Jiao, S. Sun, and J. Leng, Analysis and manufacture of an energy harvester based on a Mooney-Rivlin type dielectric elastomer, *EPL* **90**, 1303 (2010).
- [8] T. Li, S. Qu, and W. Yang, Energy harvesting of dielectric elastomer generators concerning inhomogeneous fields and viscoelastic deformation, *J. Appl. Phys.* **112**, 034119 (2012).
- [9] O. A. Araromi, I. Gavrilovich, J. Shintake, S. Rosset, M. Richard, V. Gass, and H. R. Shea, Rollable multisegment dielectric elastomer minimum energy structures for a deployable microsatellite gripper, *IEEE/ASME T. Mech.* **20**, 438 (2015).
- [10] P. Jean-Sébastien and S. Dubowsky, Large-scale failure modes of dielectric elastomer actuators, *Int. J. Solids Struct.* **43**, 7727 (2006).
- [11] X. Zhao and Z. Suo, Method to analyze electromechanical stability of dielectric elastomers, *Appl. Phys. Lett.* **91**, 061921 (2007).
- [12] J. Leng, L. Liu, Y. Liu, K. Yu, and S. Sun, Electromechanical stability of dielectric elastomer, *Appl. Phys. Lett.* **94**, 211901 (2009).
- [13] D. De Tommasi, G. Puglisi, and G. Zurlo, Electromechanical instability and oscillating deformations in electroactive polymer films, *Appl. Phys. Lett.* **102**, 011903 (2013).
- [14] D. De Tommasi, G. Puglisi, and G. Zurlo, Failure modes in electroactive polymer thin films with elastic electrodes, *J. Phys. D Appl. Phys.* **47**, 065502 (2014).
- [15] G. Zurlo, M. Destrade, D. Detommasi, and G. Puglisi, Catastrophic Thinning of Dielectric Elastomers, *Phys. Rev. Lett.* **118**, 078001 (2017).
- [16] M. Kolloche, G. Kofod, Z. Suo, and J. Zhu, Temporal evolution and instability in a viscoelastic dielectric elastomer, *J. Mech. Phys. Solids* **76**, 47 (2015).
- [17] T. Lu, L. An, J. Li, C. Yuan, and T. J. Wang, Electro-mechanical coupling bifurcation and bulging propagation in a cylindrical dielectric elastomer tube, *J. Mech. Phys. Solids* **85**, 160 (2015).
- [18] S. G. Lee, D. Y. Lee, H. S. Lim, D. H. Lee, S. Lee, and K. Cho, Switchable transparency and wetting of elastomeric smart windows, *Adv. Mater.* **22**, 5013 (2010).
- [19] C. S. Davis and A. J. Crosby, Mechanics of wrinkled surface adhesion, *Soft Matter* **7**, 5373 (2011).
- [20] K. Jun, D. Kim, S. Ryu, and K. Oh, Surface modification of anisotropic dielectric elastomer actuators with uni- and bi-axially wrinkled carbon electrodes for wettability control, *Sci. Rep.* **7**, 6091 (2017).
- [21] J. Zhu, M. Kolloche, T. Lu, G. Kofod, and Z. Suo, Two types of transitions to wrinkles in dielectric elastomers, *Soft Matter* **8**, 8840 (2012).
- [22] R. Huang and Z. Suo, Electromechanical phase transition in dielectric elastomers, *Proc. R. Soc. A-Math. Phys. Eng. Sci.* **468**, 1014 (2012).
- [23] G. Mao, X. Huang, M. Diab, T. Li, S. Qu, and W. Yang, Nucleation and propagation of voltage-driven wrinkles in an inflated dielectric elastomer balloon, *Soft Matter* **11**, 6569 (2015).
- [24] B. Li, X. Liu, L. Liu, and H. Chen, Voltage-induced crumpling of a dielectric membrane, *EPL* **112**, 56004 (2015).
- [25] G. Mao, X. Huang, M. Diab, J. Liu, and S. Qu, Controlling wrinkles on the surface of a dielectric elastomer balloon, *Extreme Mech. Lett.* **9**, 139 (2016).
- [26] X. Liu, B. Li, H. Chen, S. Jia, and J. Zhou, Voltage-induced wrinkling behavior of dielectric elastomer, *J. Appl. Polym. Sci.* **133**, 43258 (2016).
- [27] K. Li, W. Wu, Z. Jiang, and S. Cai, Voltage-induced wrinkling in a constrained annular dielectric elastomer film, *J. Appl. Mech.* **85**, 011007 (2018).
- [28] G. Mao, L. Wu, X. Liang, and S. Qu, Morphology of voltage-triggered ordered wrinkles of a dielectric elastomer sheet, *J. Appl. Mech.* **84**, 111005 (2017).
- [29] L. Shui, Y. Liu, B. Li, C. Zou, C. Tang, L. Zhu, and X. Chen, Mechanisms of electromechanical wrinkling for highly stretched substrate-free dielectric elastic membrane, *J. Mech. Phys. Solids* **122**, 520 (2019).
- [30] A. K. Srivastava and S. Basu, Mechanics of reversible wrinkling in a soft dielectric elastomer, *Phys. Rev. E* **101**, 040501 (2020).
- [31] Z. Suo, X. Zhao, and W. H. Greene, A nonlinear field theory of deformable dielectrics, *J. Mech. Phys. Solids* **56**, 467 (2008).
- [32] Z. Suo, Theory of dielectric elastomers, *Acta Mech. Solida Sin.* **23**, 549 (2010).
- [33] P. B. Xu, X. Su, J. Zhao, Y. Yu, and K. Li, Wetting of soap bubbles on soft elastomers with surface stress and gravity, *Math. Mech. Solids* **25**, 791 (2020).
- [34] E. Ventsel and T. Krauthammer, *Thin Plates and Shells: Theory, Analysis, and Applications* (Marcel Dekker Inc, New York, 2001).